Ex vivo detection and characterization of early dental caries by optical coherence tomography and Raman spectroscopy

Alex C.-T. Ko
Lin-P'ing Choo-Smith
Mark Hewko
Lorenzo Leonardi
Michael G. Sowa
National Research Council Canada
Institute for Biodiagnostics
435 Ellice Ave.
Winnipeg MB, Canada R3B 1Y6

Cecilia C. S. Dong
Peter Williams
University of Manitoba
Department of Restorative Dentistry
Faculty of Dentistry
780 Bannatyne Ave.
Winnipeg MB, Canada R3E 0W2

Blaine Cleghorn
Dalhousie University
Department of Dental Clinic Sciences
Faculty of Dentistry
5981 University Ave.
Halifax NS, Canada B3H 3J5

Abstract. Early dental caries detection will facilitate implementation of nonsurgical methods for arresting caries progression and promoting tooth remineralization. We present a method that combines optical coherence tomography (OCT) and Raman spectroscopy to provide morphological information and biochemical specificity for detecting and characterizing incipient carious lesions found in extracted human teeth. OCT imaging of tooth samples demonstrated increased light backscattering intensity at sites of carious lesions as compared to the sound enamel. The observed lesion depth on an OCT image was approximately 290 μm matching those previously documented for incipient caries. Using Raman microspectroscopy and fiber-optic-based Raman spectroscopy to characterize the caries further, spectral changes were observed in PO_4^{3-} vibrations arising from hydroxyapatite of mineralized tooth tissue. Examination of various ratios of PO_4^{3-} ν_2, ν_3, ν_4 vibrations against the ν_1 vibration showed consistent increases in carious lesions compared to sound enamel. The changes were attributed to demineralization-induced alterations of enamel crystallite morphology and/or orientation. OCT imaging is useful for screening carious sites and determining lesion depth, with Raman spectroscopy providing biochemical confirmation of caries. The combination has potential for development into a new fiber-optic diagnostic tool enabling dentists to identify early caries lesions with greater sensitivity and specificity. [DOI: 10.1117/1.1915488]

Keywords: dental caries; optical coherence tomography; Raman spectroscopy; hydroxyapatite; demineralization; fiber-optics.

Paper SS04161RR received Aug. 12, 2004; revised manuscript received Dec. 9, 2004; accepted for publication Dec. 9, 2004; published online May 26, 2005.

1 Introduction

Dental caries (i.e., dental cavities or dental decay) is a common oral disease that many people have experienced at some point in their life. With the introduction of fluoride in drinking water and toothpastes, there has been a decline in the prevalence of dental caries in Western countries.[1] However, a recent report states that caries still remains a large problem in specific population groups (e.g., minority children, the economically underprivileged, older people, the chronically ill, and institutionalized persons).[2] Further, the patterns of caries development are changing, to those with smaller lesion sizes and slower progression rates, making caries more difficult to detect with existing conventional techniques.[1] This is further complicated when caries develop at locations which are not clinically visible (e.g., between adjacent teeth). Current diagnostic methods involve subjective clinical criteria (color, ''softness,'' resistance to removal) and the use of tools such as the dental explorer and dental radiographs. Such methods may not be reliable for detecting interproximal lesions (those between adjacent teeth) because these carious lesions are not clinically visible. In addition, these clinical methods do not adequately detect changes in caries development and do not possess the sensitivity, specificity nor ability to account for the dynamic process of demineralization–remineralization.[1,2] Therefore, more refined diagnostic tools are required to identify early noncavitated carious lesions and to monitor their activity as well as severity. Early caries detection can potentially increase the implementation of conservative treatment methods centered on tooth preservation rather than restoration. Conservative methods include nonsurgical interventions such as fluoride to promote remineralization, antimicrobials to arrest caries activity, and sealants to prevent dental caries. New diagnostic techniques will enable the clinician to monitor patients for further lesion demineralization or remineralization, to evaluate the effectiveness of treatment strategies, as well as to encourage patient compliance in following sug-

Address all correspondence to L.-P. Choo-Smith, Institute for Biodiagnostics, National Research Council Canada, 435 Ellice Ave., Winnipeg, MB, Canada, R3B 1Y6. Tel: (204) 984-7517; Fax: (204) 984-5472; E-mail: lin-p'ing.choo-smith@nrc-cnrc.gc.ca

1083-3668/2005/$22.00 © 2005 SPIE

gested preventive measures. Several methods addressing the need for better early dental caries diagnostic tools with improved sensitivity and specificity have been investigated and recently reviewed.[3–6] Among the methods are direct digital radiography (DDR), digital imaging fiber-optic transillumination (DIFOTI), electroconductivity measurements (ECM), quantitative light-induced fluorescence, and laser fluorescence.[3] DDR has the capability to optimize diagnostic imaging operation by eliminating the need for film processing as well as to reduce the potential patient radiation dose. Although the technique uses a lower radiation dose, the application of the method is still limited by the ionizing radiation required to obtain an image. Like conventional radiographs, the technique provides little value in the detection of initial enamel lesions.[3] DIFOTI, marketed by Electro-Optical Sciences (Irvington, NY, USA), involves a transillumination technique through the use of a fiber-optic device to shine light on the tooth. The image captured represents the scattered and absorbed light as it traversed the tooth. Although the technique can detect incipient caries, the method is subjective, relying on the expertise of the examiner with a high level of intra- and interexaminer variability.[3,7] Another technique, ECM is based upon the observation that sound surfaces have limited or no conductivity whereas surfaces with caries will have measurable conductivity that will increase with increasing demineralization. The drawback of the technique is its lack of specificity, which limits its usefulness in deciding whether or not to treat a lesion operatively. The low specificity increases the chance of false-positive results which translate into possibly unnecessary invasive treatment.[5]

Perhaps the most advanced of the technologies available is that based on fluorescence spectroscopy. With quantitative light-induced fluorescence, light at 488 nm is shone on a tooth and induces a natural fluorescence. Areas of demineralization appear as dark spots with mineral loss correlating with a relative loss of fluorescence radiance. With this method, the presence of bacterial plaque or saliva interferes with the usefulness of the technique.[8] A related approach, laser fluorescence, uses light at 633 nm and the reflected fluorescence is measured. The light interacts with the bacterially produced porphyrins that leach into the decayed regions. Therefore fluorescence is suggestive of decay present. This is the basis for the commercially available DIAGNOdent device by KaVo (Lake Zurich, IL, USA). Recent clinical studies indicate that this latter technique can lead to false-positive results due to the presence of stains, deposits, calculus and organic material in the region of interest[9] and is not suitable for detecting initial carious changes in enamel.[10] Therefore, despite the potential of these various technologies, the methods are prone to subjectivity issues with high intra- and interexaminer variability, false-positive results due to stains or organic deposits, and the unsuitability for detecting initial enamel caries at interproximal sites. As a result of these shortcomings, more refined tools with improved sensitivity and specificity are needed for early detection of interproximal dental caries.

We propose that the combination of an optical and a spectroscopic technique, namely, optical coherence tomography and Raman spectroscopy, has the potential to be developed as a fiber-optic tool for early detection of dental caries. Optical coherence tomography (OCT) can provide morphological information for dental caries detection similar to the conventional images with which dental clinicians are familiar. Raman spectroscopy furnishes biochemical specificity because it is based on spectral peaks specific to the (bio)chemical and structural properties of tooth mineralization and not to staining or organic matter. Combining the two technologies takes advantage of their synergies for detecting lesions and for providing objective biochemical information. In so doing, the limitations of using a single method alone can be minimized and potentially overcome, thereby yielding an approach with greater sensitivity for early dental caries detection.

To better understand how OCT and Raman spectroscopy are well suited for caries detection, it is useful to examine the nature of dental caries development. In particular, the focus will be on dental caries of the enamel which is the highly mineralized tissue covering the tooth crown. Dental caries arises from the destruction of tooth structure by acid-forming bacteria found in dental plaque. The early dental carious lesion (incipient caries) is noncavitated and limited to the outer enamel surface. This caries type presents as a visible ''white spot'' when the tooth is air dried. Histological studies have shown that white spot lesions consist of four regions or layers.[11,12] The first region (the enamel surface of the incipient lesion) is intact and well mineralized. The second region which lies immediately beneath the highly mineralized surface layer is very porous (25–50% porosity by volume) and is the largest of the four regions. The third region (the dark zone) does not transmit polarized light (also known as positive birefringent) because it consists of many tiny pores as well as interprismatic areas and cross striations. The fourth or deepest region is the translucent zone. It is the advancing front of the enamel lesion and appears structureless when examined with polarized light. Compared with the subsurface, the surface zone ($\sim$30 μm thick) contains more fluoride, less water, less carbonate, is more highly mineralized and the enamel crystals are often larger and oriented differently from those below.[11] Such properties render the enamel surface more resistant to acid attack. This surface layer is also partly formed by remineralization in which dissolved ions (calcium and phosphate) originating from the subsurface region and saliva are deposited into the surface layer. The original crystalline framework of the enamel rods serves as a nucleating agent for remineralization. Depending on the extent of demineralization, enamel caries can extend from a depth of $\sim$100 to 250 μm (for incipient caries) to entirely through the enamel at which point the cavitated lesion ($\sim$1.5 mm deep) has just extended into the underlying dentin.[13] The enamel itself is an acellular tissue composed of 80–90% by volume of crystals of carbonated calcium hydroxyapatite [$Ca_{10}(PO_4)_6(OH)_2$ where PO_4^{3-} or OH^- can be substituted by CO_3^{2-}], with the remaining 10–20% being fluid and organic (mainly proteinaceous) material.[11] The carbonated apatite crystals are arranged into bundles to form rods or prisms with intercrystalline spaces between rods that allow diffusion of ions during the caries process. The structural and biochemical changes associated with enamel caries development suggest that OCT imaging and Raman spectroscopic techniques offer potential for differentiating between sound (i.e., healthy) and carious enamel.

OCT is a noninvasive technique that provides high-resolution depth imaging of near surface tissue structures. Similar to ultrasound in operation but offering an order of

magnitude of greater spatial resolution, OCT provides morphological images with 20 μm resolution to depths of ~2 mm.[14] Current dental radiographs have a resolution of 50 μm and superimpose the entire three-dimensional tooth structure onto a two-dimensional film. Dental applications of OCT have demonstrated its potential for *in vivo* imaging of intraoral tissue such as delineating structural components of gingival tissue (e.g., sulcus, epithelium, connective tissue layer) as well as hard tissue structures (e.g., enamel, dentin and the dentin–enamel junction).[14–17] More recently, polarization sensitive OCT (PS-OCT) with near-infrared excitation has been used to image dental carious lesions and has demonstrated the potential of the technique for monitoring the progression of lesions over time.[15,17–19] OCT is therefore well suited for detecting morphological changes in teeth arising from caries formation. Our approach of combining Raman spectroscopy with OCT will add biochemical specificity providing important information for resolving the structural features observed with OCT imaging thereby reducing false-positive observations.

Raman spectroscopy is a vibrational spectroscopic technique that provides details on the biochemical composition, molecular structure, and molecular interaction in cells and tissues.[20] Highly specific biochemical information about proteins, lipids, carbohydrates, nucleic acids and in this case, mineral orientation and composition (e.g., PO_4^{3-}, CO_3^{2-}), can be obtained.[21,22] Raman spectroscopy is well suited to examine mineralized tissues and has been used previously by various research groups to study bone and teeth; for example to understand the mechanical properties of bone, mineralization of hydroxyapatite, and the effects of postextraction treatment of teeth.[21–28] Earlier studies characterizing dentin and enamel structures and their interfaces with resin and bonding agents, have shown that Raman spectra of tooth enamel and dentin exhibit peaks characteristic of the inorganic (i.e., hydroxyapatite) and organic (e.g., collagen in dentin) components of teeth as well as quantitative chemical information of the adhesive interface.[29–35] Polarized Raman spectroscopy used to study the fundamental structural characteristics of tooth enamel crystallites have observed differences due to crystal orientation.[36,37] The application of near-infrared (785 nm) fiber-optic Raman spectroscopy to characterize advanced dental caries has shown spectral differences between sound and carious regions of teeth based upon Raman peaks superimposed on a broad luminescence background of unknown origin.[38,39] The background fluorescence is problematic for Raman spectroscopy, often masking peaks of interest and is not a solid basis for differentiating healthy from carious teeth. Fluorescence changes might arise from stains and food particles trapped within the carious regions. In our studies, the strengths of the biochemical specificity of Raman spectroscopy will be used by examining spectral peaks characteristic of hydroxyapatite within mineralized dental tissue.

We describe our various studies using OCT and Raman spectroscopy to detect and characterize early enamel carious lesions in extracted human teeth. Comparisons will be made with results obtained from sound tooth enamel. The Raman studies are conducted with microspectroscopy, polarized Raman spectroscopy, and fiber-optic sampling to illustrate the similarity of the information obtained with both (microscopy and fiber-optic) measurement modes and the potential of developing the Raman technique combined with OCT, into a fiber-based tool for clinical applications with improved sensitivity and specificity.

2 Materials and Methods

2.1 *Tooth Samples and Chemicals*

Human premolars ($n=15$) were collected from orthodontic patients at the Dental Clinic of the Faculty of Dentistry, University of Manitoba. Approvals from the human ethics committees of the Institute for Biodiagnostics (National Research Council Canada), University of Manitoba and Dalhousie University were obtained prior to sample collection. All teeth were examined in patients before extraction and no discoloration of the marginal ridge was observed. Remaining soft tissue on extracted teeth was removed by scaling and the samples were thoroughly rinsed with water. Teeth were preserved in sterile filtered de-ionized water until measurement. Each tooth sample was radiographed and independently reassessed *ex vivo* by two clinical investigators at the University of Manitoba and Dalhousie University, respectively. Control caries-free teeth had no visible decalcification or demineralization. Incipient carious teeth included regions of decalcification with intact surfaces and opacity of enamel. Among the 15 extracted teeth, 10 were identified to be carious teeth with at least 15 caries sites in total. The teeth were used for spectroscopic measurements without any treatment. Synthetic hydroxyapatite in powder form was obtained from Sigma-Aldrich Inc. (St. Louis, MO, USA) and used for confirmation of Raman spectral peak assignments of hydroxyapatite within tooth enamel.

2.2 *Optical Coherence Tomography*

Optical coherence tomography image slices were acquired on an OCT-2000 system with software Revision A (Humphrey Systems, Dublin, CA, USA) and equipped with a superluminescent diode source. The source has a central wavelength of 850 nm and the laser spot size is 10–20 μm. The optical power at the sample was 750 μW for all image sets. Both the axial and transverse resolutions were 10–20 μm. The OCT-2000 system has an x–y galvanometer pair for beam steering and an integrated camera for sample viewing during data collection. For image acquisition, the galvanometer pair was limited to straight-line collection only. The shortest lateral scan length (~2.0 mm) of the system was used to provide images of high pixel density. The scan rate was 100 A scans/s.

For these *ex vivo* studies, tooth samples were imaged in an upright position by affixing the apical root portion of the tooth to the microscope slide using dental rope wax. The samples were imaged using a free-space coupled arrangement. The laser line was focused to the thinnest line on the sample image and during acquisition, the polarization was matched to the sample in order to optimize the OCT signal strength. OCT data were exported into MATLAB (The Mathworks Inc., Natick, MA, USA) and interpolated using a bilinear filter method within MATLAB to generate false-color images. The scan length was corrected for nonophthalmologic uses of the system by imaging a linear scale. The depth distance was corrected by dividing the depth obtained from the system (assuming imaging in air) by a value of 1.6, the refractive index of tooth enamel.[40]

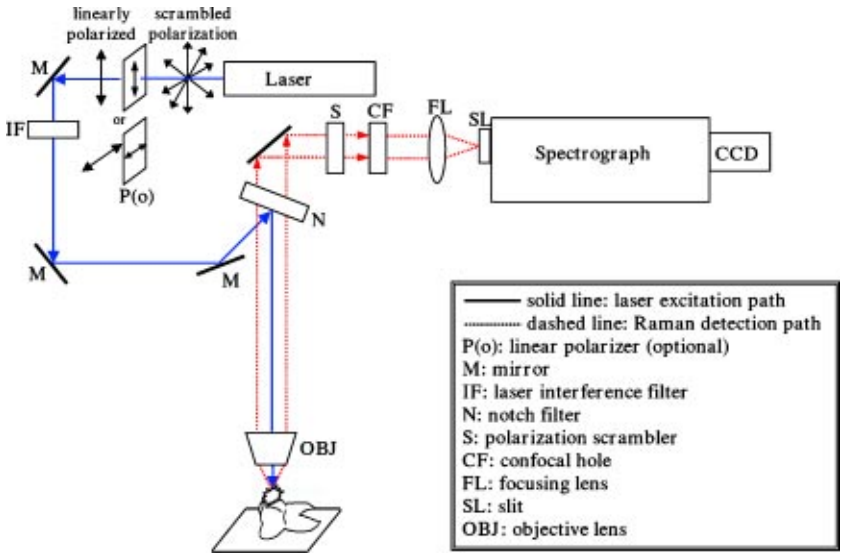

Fig. 1 Schematic diagram of the Raman microspectroscopic system illustrating the laser excitation (solid line) and Raman signal detection (dashed line) paths for acquiring tooth spectra in a 180° geometry. Abbreviations are provided in the inset for each optical element. The linear polarizer (P) is only used when performing polarized Raman experiments.

2.3 *Raman Microspectroscopy and Fiber-Optic Raman Spectroscopy*

Raman spectra were acquired on a LabRamHR confocal Raman microspectrometer (Horiba Jobin Yvon, Edison, NJ, USA) operating with near-infrared laser excitation at 830 nm (Lynx series TEC 100 diode laser, Sacher Lasertechnik GmbH, Marburg, Germany), (Fig. 1). In brief, the Raman microspectrometer consists of an Olympus BX41 microscope equipped with a motorized XYZ stage, a spectrograph with 300 lines/mm grating and an air-cooled CCD detector optimized for the NIR region. Spectra were also acquired using a fiber-optic Raman probe (830 nm excitation, InPhotonics, MA, USA) that was interfaced to the LabRamHR spectrometer. Laser powers at the sample were 24, 39, 54, 48, and 52 mW under ×100 (Olympus LMPlan IR), ×50 (Olympus MPlan), ×10 (Nikon), and ×5 (Leica HC PL Fluotar) microscope objectives and fiber-optic probe, respectively. For microspectroscopy, the confocal hole size was set at 800 μm and the slit size at 100 μm. The spectral resolution was 4 cm^{-1} for the spectra acquired with the microscope objectives and 7 cm^{-1} for the fiber-optic probe. These values were determined using an 841 nm neon line. A polarization scrambler is placed in the Raman collection path in order to eliminate potential artifacts from polarization-sensitive components (e.g., diffraction grating) (Fig. 1). LABSPEC (version 4.12, Horiba Jobin Yvon, Edison, NJ, USA) software accompanying the LabRamHR system was used for spectrometer control and data acquisition. For Raman microspectroscopy, the tooth surface not being studied was placed lying on a microscope slide and then secured with dental wax. Wax was applied only at the apical root to avoid wax contamination at the surfaces of interest. Tooth surfaces to be examined were positioned approximately normal to the laser beam (Fig. 1). For fiber-optic sampling, tooth samples were positioned upright on a microscope slide and the fiber-optic probe was placed at a position 5 mm away (optimal laser focus) from the tooth surface. The sampling position was optimized by a XYZ translator assembled in-house. A camera coupled with an ×10 objective lens was used for monitoring the positioning and for capturing photomicrographs of the sampled locations.

For our studies, the orientation of the enamel crystals within tooth samples were defined with respect to the laser beam as has been described by Tsuda and Arends.[36] Raman spectra obtained from the cross-sectioned surface of longitudinally sectioned (i.e., crown to root direction) tooth samples were defined as acquired in a transverse excitation/detection mode [Fig. 2(A)]. Raman spectra recorded from unsectioned whole tooth were defined as acquired in a normal excitation/detection mode [Fig. 2(B)]. Spectra were measured using 30 s acquisition time with 15 accumulations for the ×5 objective or 15 s acquisition time with 15 accumulations for the other objectives and the fiber-optic probe in order to generate spectra of good signal to noise ratios. For point mapping experiments using the ×10 objective, the laser spot size was about 37×25 μm^2. Spectra were acquired at 140 μm steps along the *x* axis and 113 μm steps along the *y* axis resulting in a 10×10 array map covering an area of 1260×1017 μm^2.

Polarized Raman microspectroscopic measurements of tooth samples were acquired by placing a NIR (780–1250 nm range) linear polarizer (Melles Griot, Irvine, CA, USA) in the laser excitation path after the radiation exits the laser head (Fig. 1) to obtain linearly polarized light from the originally scrambled laser polarization (Lynx series TEC 100, Sacher Lasertechnik GmbH, Marburg, Germany). One set of measurements was acquired with the linear polarizer in one orientation and a subsequent set of measurements was acquired with the linear polarizer rotated 90° such that the second polarization direction is orthogonal to the first polarization direction. All other measurement conditions (e.g., optics, sample orientation, etc.) were left unchanged between the two measurement sets. Similar to the other nonpolarized measurements, a polarization scrambler is placed in the Raman collection path in order to eliminate potential artifacts from polarization-sensitive components.

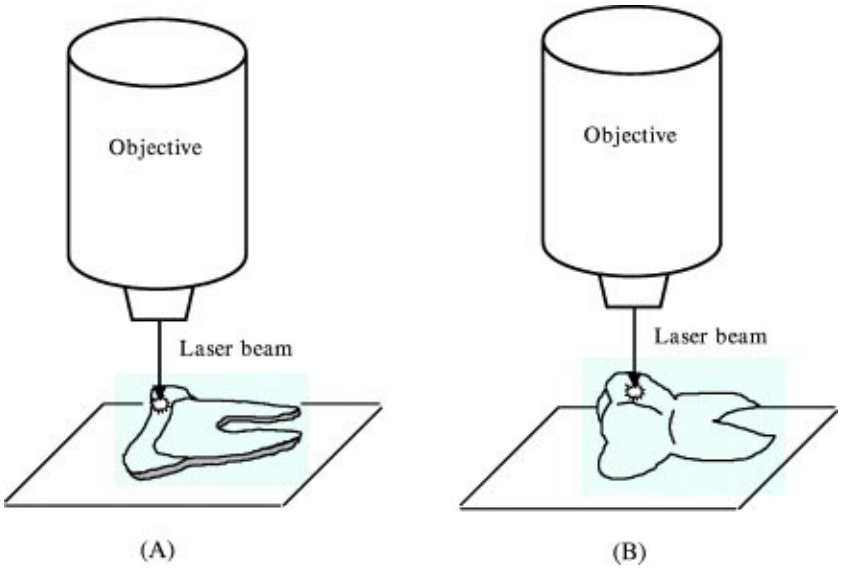

Fig. 2 Diagrammatic representation of the two spectral acquisition configurations using (A) transverse excitation/detection on a longitudinally sectioned (crown to root direction) tooth, and (B) normal excitation/detection on an unsectioned whole tooth. Drawing illustrates the actual sample orientation under the microscope objective.

2.4 *Raman Spectroscopic Data Analysis*

Background Raman spectrum, acquired with no sample in place and with all other experimental conditions unchanged, was subtracted from sample spectra to correct for background signal arising from optical elements in the laser path. The spectrum of a luminescent green glass reference, calibrated previously with a NIST traceable reference tungsten halogen lamp (The Eppley Laboratory, Inc., Newport, RI, USA) of known temperature, was used to correct the sample spectra for the instrument response function.[41–43] The majority of the Raman spectra (sound enamel and carious enamel) acquired contained a minor sloping baseline as the background [Fig. 3(A)]. A few spectra of carious enamel contained a large background fluorescence [Fig. 3(B)]. For semiquantitative spectral analyses and mapping experiments, the spectra were first baseline corrected using a sixth order polynomial fit through the spectra at 375, 512, 700, 840, 1200, and 1400 cm^{-1}. Figure 3 illustrates representative spectra before and after the backgrounds were removed by subtracting the fit of the sixth order polynomial. The corrected spectra were then normalized to the 959 cm^{-1} peak. Peak ratios were determined by taking the intensities of the various Raman bands of interest. In a similar approach, an intensity ratio map was generated from the mapping data. The resulting Raman map presented was smoothed using the bilinear interpolation method for two-dimensional data in MATLAB.

3 Results and Discussions

3.1 *Optical Coherence Tomography of Dental Caries*

Figure 4 shows representative false-color OCT images obtained from a sound tooth and a tooth surface containing two clinically confirmed incipient lesions also known as white spots. The images present the lateral scan position versus the imaging depth with higher intensity correlating with greater light backscattering. In the image of the sound tooth [Fig. 4(A)], an intense light backscattering is observed at the tooth surface. This represents the scattering of the light due to the change of refractive index as the light transitions from air to the tooth enamel surface. For the sound surface, beyond the initial first few microns, the light backscattering rapidly decays with no further changes in intensity deeper into the enamel. This image suggests that the surface is intact with no structural defects, increased porosity or loss of mineral structure. There is no evidence of a further scattering boundary deeper into the tooth that would suggest the presence of the dentin–enamel junction (DEJ). This feature, however, has been observed by other groups performing OCT imaging of tooth.[14,16] The absence of an observable scattering boundary representing the DEJ on our images is possibly due to the large enamel thickness observed at the region sampled and the attenuation of the scattered signal as it penetrates the enamel; enamel is known to weakly scatter near-infrared light (850 nm in our studies).[40] Other OCT images acquired of the enamel closer to the cemento–enamel junction (i.e., borderline between the crown and root complex) have demonstrated the DEJ (figure not shown for brevity). Therefore, it is likely the enamel thickness that limits the observation of the DEJ in our OCT images. In contrast to the image of the sound enamel surface, the image [Fig. 4(B)], taken of the carious sites portrays diffuse scattering in two triangular-shaped zones immediately below the surface areas. Once again there is intense light backscattering at the tooth surface indicating that the incipient lesions have intact surfaces. The diffuse scattering intensity in the region below the surface is due to the occurrence of multiple scattering and indicative of an area of higher porosity within an otherwise dense enamel structure. This suggests that demineralization has occurred below the intact surface as occurs with early dental caries formation. Similar imaging results were reported by Fried et al.[19] using PS-OCT on natural interproximal lesions. Based on the OCT image, it is estimated that the deepest area of the lesions is approxi-

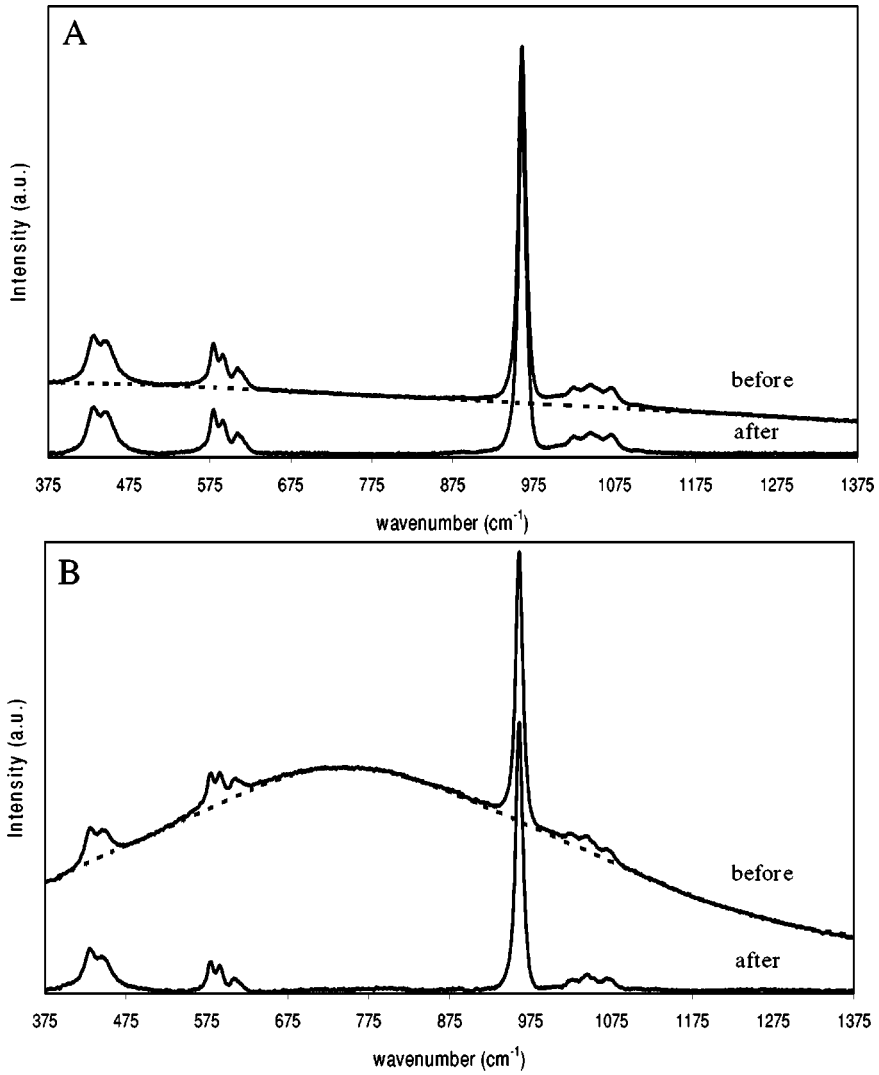

Fig. 3 Representative Raman spectra illustrating the background fluorescence acquired from (A) the majority of sound and carious dental enamel and (B) from a few number of carious sites. For both panels, the upper solid traces illustrate the original spectrum. The dashed traces are the sixth order polynomial fits that were used for correction and the lower solid traces are the results after subtracting the polynomial fits of the background fluorescence.

mately 290 μm deep. The triangular-shaped region below the surface and this depth estimation is consistent with histological studies in the literature that have shown a similar triangular-shaped lesion body with 100–250 μm depth typical of ''white spot'' carious lesions.[11–13] OCT is able to provide morphological information of near-surface tissue structures and defects and is particularly sensitive to changes in refractive index as the light interacts with the sample. It is therefore a good first approach for examining tooth samples to screen for early dental caries and estimating the lesion depth. From a clinical perspective, lesion depth is useful for determining the extent of caries activity and in aiding the decision to surgically restore or promote remineralization. In addition, the depth can be used to monitor remineralization and to evaluate the arrest of further caries progression.

3.2 *Raman Microspectroscopy of Sound and Carious Enamel*

Following the identification of a possible carious lesion by OCT, false-positive results can be reduced by confirming the presence of caries using Raman spectroscopic characterization. Figure 5 illustrates representative Raman spectra, obtained with an $\times 10$ objective, of sound enamel and carious enamel, both from unsectioned whole teeth, and of synthetic hydroxyapatite (OHAp). The major band positions and tentative assignments of enamel and OHAp spectra are summarized in Table 1 and are compared with those previously reported. Our Raman spectra show good agreement with the literature values in terms of the respective Raman shifts. An examination of the Raman spectra from sound and carious enamel revealed differences in the relative band intensities of various Raman peaks, however, no new bands, band shifts, or disappearance of bands were evident. The symmetric stretching vibration (ν_1 mode) of phosphate (PO_4^{3-}) at 959 cm^{-1} dominates both sound and carious enamel spectra. The peak position is characteristic of carbonated biological apatite found in bone, dentin and enamel.[21,24,29] A similar peak in the spectrum of synthetic hydroxyapatite has a peak maximum at 962 cm^{-1}. The higher Raman shift of this peak indicates a

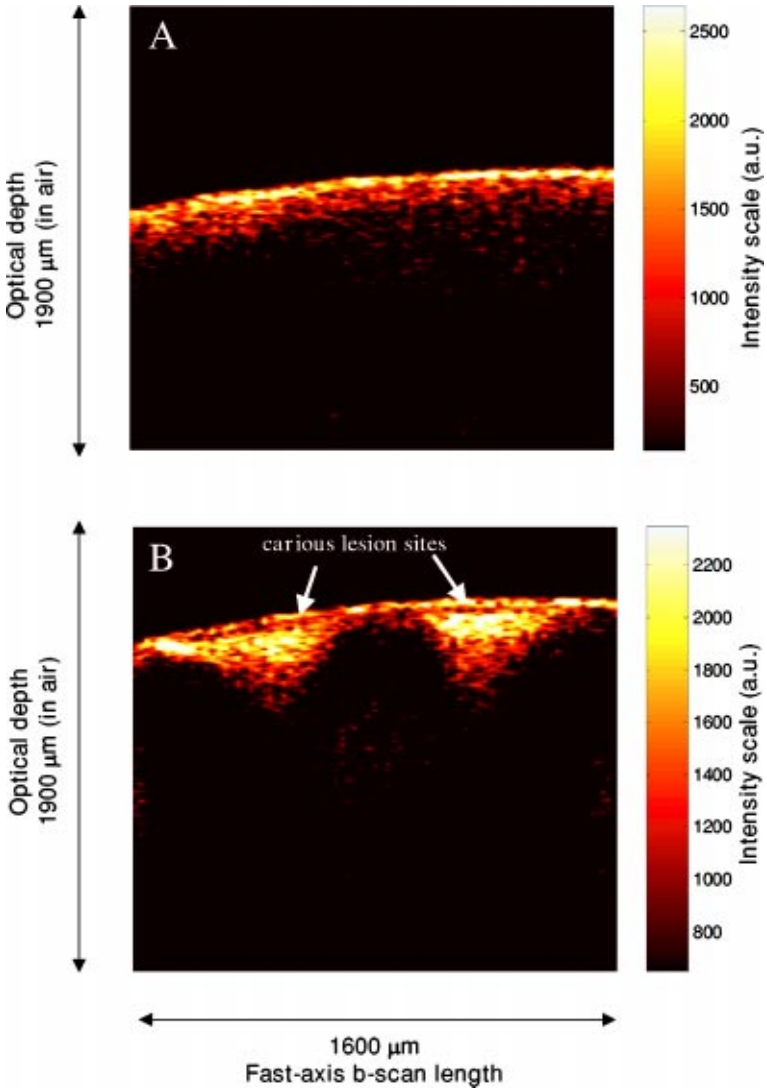

Fig. 4 Representative false-color OCT images of lateral scan length as a function of depth from (A) sound enamel tooth surface (minimum light back scattering with depth) and (B) carious enamel surface containing two lesions (significant light backscattering). The carious lesion sites are indicated with the arrows.

higher crystallinity of the synthetic hydroxyapatite as compared to carbonated hydroxyapatite. In carbonated hydroxyapatite, CO_3^{2-} has been known to substitute PO_4^{3-} yielding type-B carbonated hydroxyapatite; in type-A CO_3^{2-} substitution, the OH^- is replaced in the hydroxyapatite crystal.[44,45] The incorporation of CO_3^{2-} into the hydroxyapatite crystal deforms the crystal structure causing a decrease in crystallinity. There was no obvious change in the full-width at half-maximum (FWHM) of the 959 cm^{-1} peak between sound and carious enamel spectra. The FWHM is $\sim 10.0 \pm 0.24$ cm^{-1} and corresponds to earlier studies that have examined the FWHM of enamel.[46] Studies involving infrared absorption and Raman studies have reported the broadening of this peak upon incorporation of CO_3^{2-} (type-B) into synthetic hydroxyapatite.[47,48] Since an early event of demineralization is the dissolution of CO_3^{2-} by acid attack,[49] one might expect the spectra of carious lesions to have an increased $\nu_1\, PO_4^{3-}$ Raman shift and decreased peak width compared to spectra of sound enamel. Both of these features would be indicative of increased hydroxyapatite crystallinity. Such changes were not observed. Our studies involve biological hydroxyapatite, however, the crystallinity differences reported in the literature were from studies involving synthetic hydroxyapatite crystals.

An examination of the 1069 cm^{-1} peak assigned to both PO_4^{3-} and type-B CO_3^{2-} of apatite also show no obvious changes between sound and carious enamel despite the loss of carbonate with demineralization. Chemical analyses of different histological zones of the enamel lesion showed a carbonate level of 1–2% (wt/wt) in the lesion body compared to an average of 2% (wt/wt) in the outside layers of sound enamel.[50,51] It is not surprising that Raman spectroscopy is unable to detect the difference at this low concentration level. Spectral analyses is further complicated by the fact that the peak at 1069 cm^{-1} is a combination of PO_4^{3-} and type-B CO_3^{2-} vibrations.

In spite of these findings, changes are visibly observed with the formation of white spot lesions. There should then be some underlying biochemical or structural alterations giving

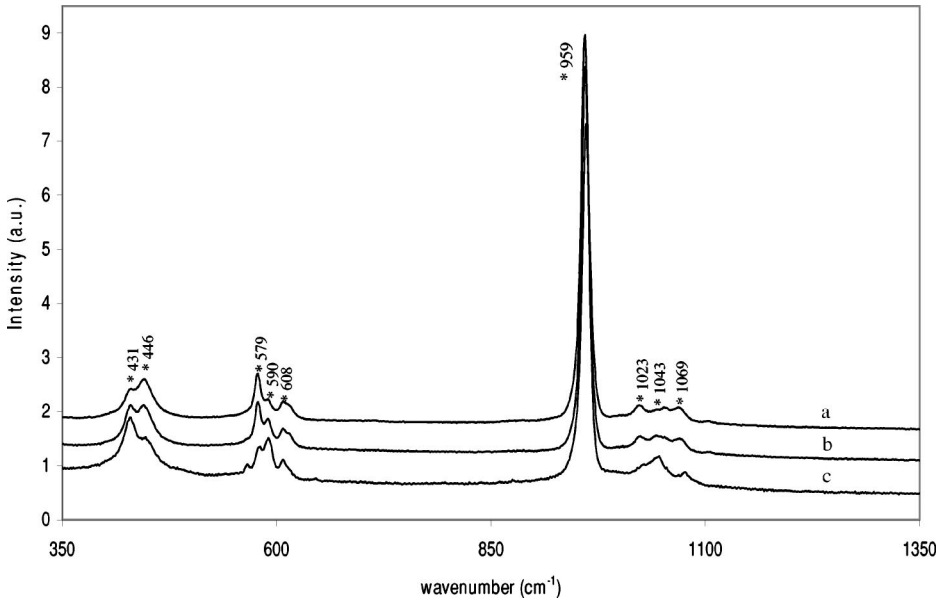

Fig. 5 Representative microspectroscopic Raman spectra of (a) sound human enamel, (b) carious human tooth enamel and (c) synthetic hydroxyapatite (OHAp) acquired with ×10 objective. Spectra are offset for clarity. The asterisks indicate peak positions. See discussion for further details.

rise to the clinically detected differences. The various other phosphate peaks were therefore examined more closely. In particular, peak intensity ratios were determined to be a better method for interpreting such spectroscopic data. This approach was chosen since Raman spectroscopy is known for its sensitivity toward sampling geometry such as laser focusing distance, sampling angles and the topography of the sample surface. This is especially true for (confocal) Raman microspectroscopy where the sampling volume is very small and any minor variations in sampling condition can alter the collection efficiency, thus affecting the signal intensity.

Figure 6 shows representative Raman spectra of sound and carious enamel in the regions of 350–700 cm^{-1} [Fig. 6(A)] and 800–1200 cm^{-1} [Fig. 6(B)]. Symmetric bending vibrations (ν_2 mode) of PO_4^{3-} give rise to two major peaks at 431 and 446 cm^{-1}. In the sound enamel spectrum, the 446 cm^{-1} peak has a greater intensity than the 431 cm^{-1} peak. These two bands are also present in the caries spectra, however, their relative intensities are reversed with the 431 cm^{-1} peak intensity greater than the 446 cm^{-1} peak. A series of bands at 579, 590, 608, and 614 cm^{-1} (shoulder band) are assigned to asymmetric bending vibrations (ν_4 mode) of PO_4^{3-}. The band pair at 579 and 590 cm^{-1} shows an intensity profile change similar to that observed for the ν_2 mode with the 590 cm^{-1} band of greater intensity in the caries spectrum but weaker intensity in the sound enamel spectrum. The two bands at 608 and 614 cm^{-1} do not demonstrate obvious changes between sound and carious enamel spectra. The asymmetric stretching vibration (ν_3 mode) of PO_4^{3-} constitutes a more complicated region of the spectra [Fig. 6(B)]. Raman bands were observed at 1023, 1043, 1052, and 1069 cm^{-1}. The intensity of the 1043 cm^{-1} band increases noticeably in the caries spectrum whereas the other three bands do not show prominent intensity variations. The numerous tooth samples examined showed various degrees of spectral change between sound and carious sites, however, the bands at 431, 590, and 1043 cm^{-1} showed consistent characteristic differences. These changes are highlighted in Fig. 7(B) where the intensity ratios of various bands relative to the 959 cm^{-1} band are plotted against sampling locations indicated in the photomicrograph of Fig. 7(A). This figure depicts an enamel surface containing a carious lesion. The carious lesion appears as a white area on the image with the marked dots representing various sampling locations. The intensity ratio plot shows enhanced 431, 590, and 1043 cm^{-1} bands relative to the 959 cm^{-1} band at the carious lesion whereas the other bands do not show significant intensity changes. The same finding is observed in the Raman intensity ratio image map based upon the 1043 cm^{-1}/959 cm^{-1} peaks obtained from a 10×10 point mapping study [Fig. 7(C)]. Both the size and the location of the carious lesion on the Raman map match very well with the photomicrograph. This result further confirms the validity of the Raman bands selected for caries detection. Overall, the findings of Fig. 7 describe a method of contrasting sound and carious enamel based upon Raman signal intensity ratios of various PO_4^{3-} vibrations. Hill and Petrou[39] have previously reported that carious lesions can be distinguished from sound enamel based on their Raman spectra. However their method was not fully based on the enamel's intrinsic Raman signal but rather on the level of the luminescence background upon illumination with 785 nm laser excitation. For the most part, our studies using laser excitation further to the near-infrared region (830 nm) did not show any significant background luminescence. A similar reduction of background fluorescence was also apparent in spectra acquired by Hill and Petrou in an earlier study using 1064 nm laser excitation.[38] Therein, the study focused on the 960 cm^{-1} peak as well as the 930 and 1900 cm^{-1} peak intensities for evaluation of the luminescence background.

In order to determine a rationale for the characteristic intensity changes observed at 431, 590, and 1043 cm^{-1} between sound and carious enamel, we compared our spectra more closely with those reported in the literature. It was noted that

Table 1 Raman peak positions and tentative band assignments of human tooth enamel and synthetic hydroxyapatite (OHAp) compared with previous studies in the literature.

	OHAp*	OHAp†	OHAp‡	Enamel*	Enamel§	Enamel†	Enamel‡	Enamel‖
$\nu_2\ PO_4^{3-}$	430	432	433	431	431	430	433	430
	447	449	448	446	446	446	450	448
$\nu_4\ PO_4^{3-}$	581	581	580	579	582	577	579	581
	591	593	591	590	589	590	588	590
	608	609	607	608	608	606	608	609
		617	614	614		615		
$\nu_1\ PO_4^{3}$	962	962	964	959	961	959	959	960
$\nu_3\ PO_4^{3-}$	1029	1028	1029	1023	1023	1024	1026	1032
		1043	1041					1041
	1046	1048	1048	1043	1042	1043	1043	1045
		1055	1057	1052		1050		
			1064					
	1076	1077	1077	1069	1070	1070	1071	1071
type-A $\nu_1 CO_3^{2-}$				1104	1104		1103	
type-B $\nu_1 CO_3^{2-}$				1069	1070	1071	1071	

* Raman microspectroscopy, current study.

† Reference 36.

‡ Reference 44.

§ Fiber-optic Raman spectroscopy, current study.

‖ Reference 22.

our Raman spectra of sound enamel from whole unsectioned teeth did not have the same relative peak intensities as reported in the literature of sound enamel from cross-sectioned tooth samples. The difference between these studies lies in the sampling configuration in which Raman spectra were acquired. Representative Raman microspectroscopic data of sound tooth enamel measured using two different sampling geometries are shown in Fig. 8. The upper spectrum was acquired on a longitudinally sectioned tooth sample and known as a transverse excitation/detection (exc./det.) mode whereas the lower spectrum was acquired on an unsectioned whole tooth termed the normal exc./det. mode. The transverse and the normal sampling arrangements are demonstrated in Fig. 2 and in the inset in Fig. 8. These two spectra show differences in several band intensities, which are highlighted with asterisks. The transverse spectrum differs from the normal spectrum with relatively higher Raman signal intensities at 431, 590, and 1043 cm^{-1}. These same intensity differences were also observed between sound enamel spectra and carious enamel spectra when measured using a normal exc./det. configuration. The spectrum of carious enamel measured in the normal exc./det. configuration is an intermediate between the spectra of sound enamel measured with the two sampling geometries, transverse versus normal. Considering that the biochemical composition does not change when the sampling arrangement has changed and given that the Raman signal is sensitive to both the (bio)chemical composition and structure of the sample, it is believed that the spectral differences between the two measurement configurations and between sound and carious enamel arise from structural characteristics of the enamel rods.[36,37] Tooth histology indicates that hydroxyapatite crystals are bundled into long rods with ~4–7 μm diameter.[49,52] A small portion of the enamel rods are randomly oriented but the majority are highly oriented within the enamel layer with their *c* axis (the longer axis) approximately perpendicular to the natural tooth surface.[36,49] This orientation is observed on the entire crown surface, i.e., at the top (occlusal or incisal surface) and at the sides (proximal surfaces) of the tooth crown.[49] Previous polarized Raman studies have indicated that changes in the spectral profile of enamel crystals reflect changes in the *c*-axis orientation.[36,37] Therefore, we propose that the spectral differences observed between sound and carious enamel are due to the hydroxyapatite crystallite orientation in the enamel. The demineralization process of caries formation results in changes of the enamel crystallite morphology or a loss of preferred enamel crystallite orientation which is reflected in the Raman spectrum. Polarized Raman spectroscopy has been shown to be useful in determining the enamel crystallite orientation and the structural symmetry.[36,37] Preliminary polarized Raman studies on sound

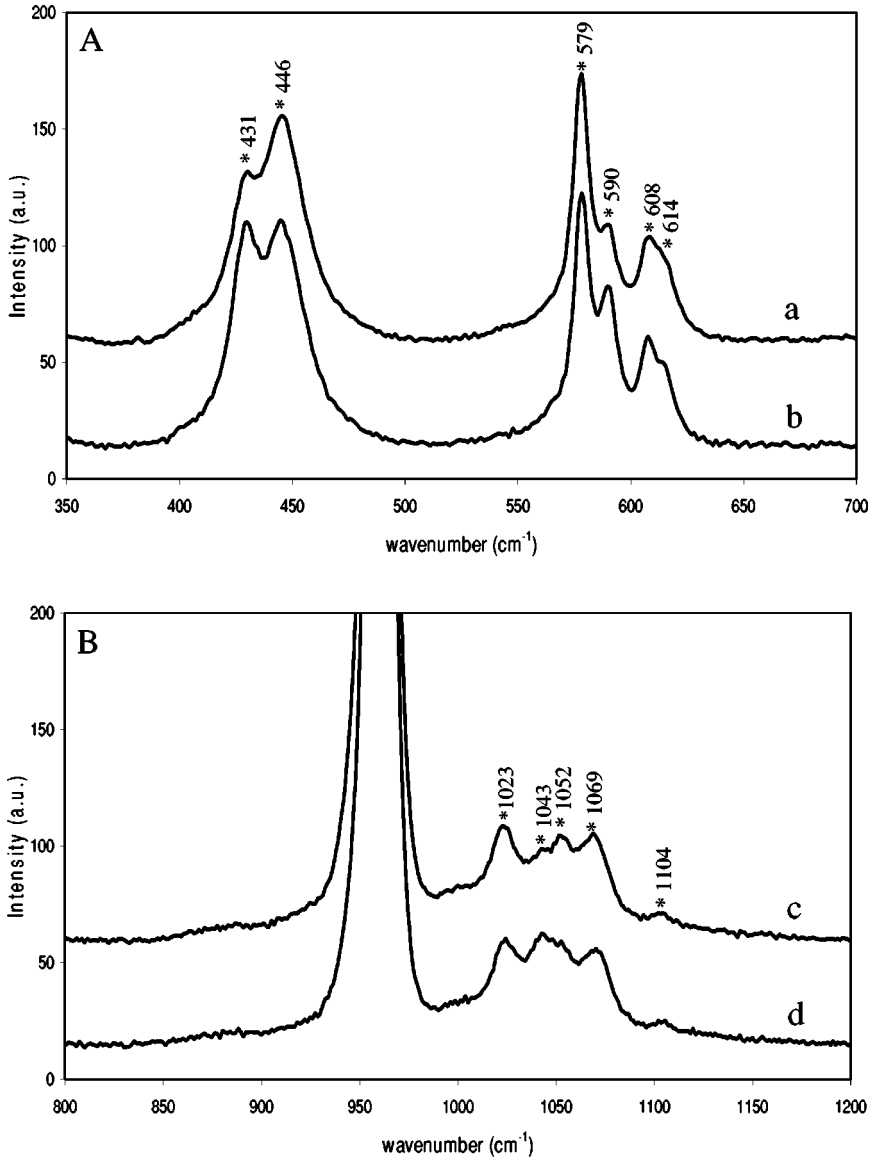

Fig. 6 Representative microspectroscopic Raman spectra in the region of (A) 350–700 cm^{-1} and (B) 800–1200 cm^{-1} of sound enamel (a and c) and carious enamel (b and d). Spectra were acquired with ×10 objective and offset for clarity. The asterisks indicate peak positions.

and carious enamel were performed to explore the hypothesis that demineralization results in alterations in enamel crystal orientation. Figure 9 shows representative polarized Raman spectra of sound enamel (traces a & b) and carious enamel (traces c & d) acquired with the linear polarizer at one polarization orientation (traces a & c) compared to the orthogonal polarization orientation (traces b & d). It is observed that the intensity of the phosphate ν_2 (431 cm^{-1}), ν_4 (590 cm^{-1}), and ν_3 (1043 cm^{-1}) peaks of sound enamel alters with the change in the polarization direction of the laser excitation. These peaks are therefore sensitive to the change in laser polarization suggesting that sound enamel is optically anisotropic. In contrast, these same peaks in Raman spectra of carious lesions do not change significantly when the laser polarization direction is rotated. Therefore the peaks are much less sensitive to the changes in laser polarization and this indicates that carious enamel is optically isotropic due to scrambling of the hydroxyapatite crystallite orientation upon demineralization. These observations support the suggestion that crystallite structural orientation changes are responsible for the spectral changes observed between sound and carious enamel.

3.3 *Fiber-Optic Raman Spectroscopy of Sound and Carious Enamel*

So far, we have demonstrated that carious enamel can be distinguished from sound enamel at the microspectroscopic level using the intensity changes of the hydroxyapatite Raman bands. We proceeded to investigate the suitability of a fiber-optic Raman probe for caries detection. Representative fiber-optic Raman spectra (not corrected for background fluorescence) of carious and sound tooth are illustrated in Fig. 10 with band assignments listed in Table 1. The major bands identified in spectra acquired with the fiber-optic probe corre-

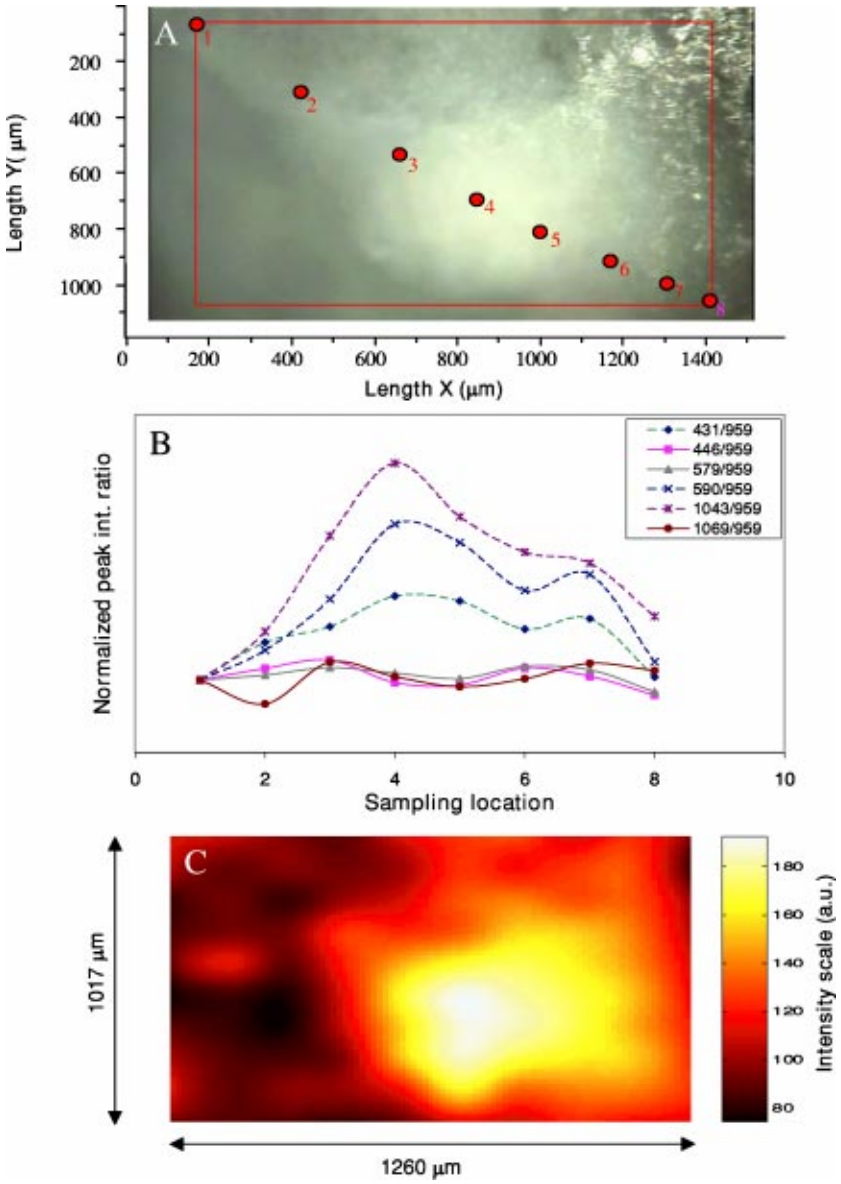

Fig. 7 (A) Photomicrograph of a human enamel tooth surface containing a carious lesion (white area). The shaded dots represent the sampling locations of the spectra acquired across the surface and used to generate (B) the peak intensity ratio plot of various phosphate peaks relative to the 959 cm^{-1} peak. (C) Raman 2-D image map of the same lesion area illustrated in (A). The smoothed Raman spectral imaging map was generated using the intensity ratios of the 1043 cm^{-1}/959 cm^{-1} peaks and plotted as a function of the 10×10 point mapping array. (See Sec. 2 for details.)

spond well to those observed from microspectroscopy. The overall spectral pattern of the fiber probe spectra resembles that of the microspectroscopic spectra. However, a slightly higher level of background luminescence is observed with the spectra possessing lower spectral resolution (~7 cm^{-1}) as shown by the unresolved peak at 1053 cm^{-1}. Comparing sound enamel and carious enamel spectra, similar increases in Raman peak intensities at 433, 590, and 1043 cm^{-1} are detected using a fiber-optic probe as with Raman microspectroscopy. The degree of changes is however less than that detected with the microscope objective and is likely the result of a larger sampling depth obtained by the fiber probe. The larger sampling depth obtained with the fiber probe indicates that the region beyond the caries lesion and into the healthy enamel layer was possibly measured in the Raman spectra. As such, any spectral contribution from the carious lesion is gradually diminished in the overall spectrum in turn resulting in slightly decreased degree of spectral discrimination between sound and carious enamel.

The greater sampling depth of the fiber-optic probe is also supported by the observation of a more intense band at 1070 cm^{-1} for fiber probe spectra compared to spectra acquired by microscopy. As mentioned earlier, this peak arises from PO_4^{3-} and type-B CO_3^{2-} of hydroxyapatite. Carbonate content is known to increase within the tooth progressing from the enamel surface to the DEJ where it reaches its maximum.[29,49,53] In Fig. 11, we present Raman microspectroscopy spectra measured of sound whole tooth enamel with a series of increasing magnification microscope objective (×5,

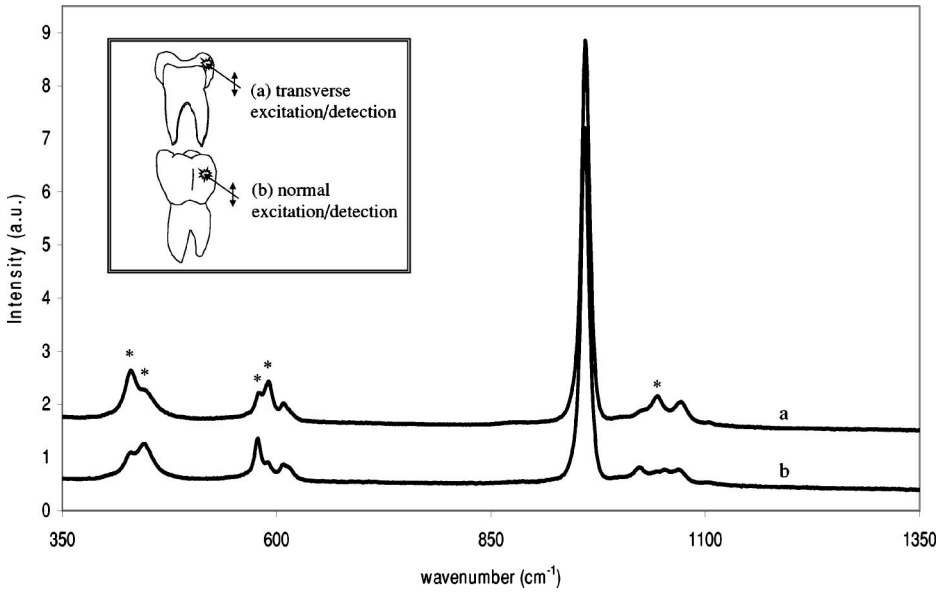

Fig. 8 Representative microspectroscopic Raman spectra of human tooth enamel using (a) transverse exc./det. configuration and (b) normal exc./det. sampling mode configuration. Measurements were acquired with a ×10 objective. Peaks highlighted with asterisks show major intensity differences between the two sampling modes. Inset: schematic illustrations of transverse (sectioned tooth) and normal (whole tooth) exc./det. sampling arrangements. Laser beam is 90° to the sample's surface in both cases.

×10,×50,×100) with increasing numerical apertures and therefore decreasing sampling volumes. Focusing on the 750–1200 cm^{-1} region, we observe that the CO_3^{2-} intensity at 1069 cm^{-1} is indeed decreasing continuously from the ×5 spectrum to the ×100 spectrum. The results with a low magnification objective and the fiber-optic data are in agreement with the known rise in carbonate content deeper into the tooth crown.

The larger sampling depth of the Raman fiber probe resulted in a slight decrease in the spectral differences between sound and carious enamel. For this reason then, it is desirable to use a fiber probe with pseudoconfocal arrangement where the measurement volume more closely approximates that of the ×10 microscope objective. With such sampling depths, healthy and early decaying enamel can readily be distinguished. Although useful for characterizing and confirming demineralization, using such a Raman probe alone would not be practical for screening in order to locate possible carious sites. The small sampling of Raman point spectroscopy would result in a greater chance of missing the lesion. For this reason, it is beneficial to couple OCT imaging with Raman spectroscopy. For the purposes of detecting suspicious carious sites, OCT would be useful for rapidly screening larger areas than that interrogated with the Raman probe. The region cov-

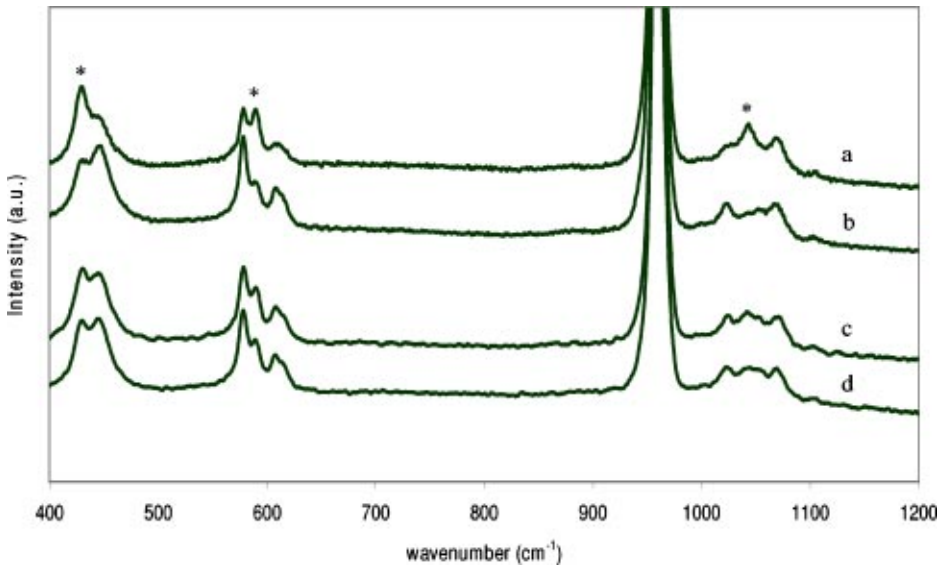

Fig. 9 Representative polarized Raman spectra of sound enamel (a and b) and carious enamel (c and d) acquired with the linear polarizer in one polarization direction (a and c) and the orthogonal polarization orientation (b and d). The asterisks highlight peak positions.

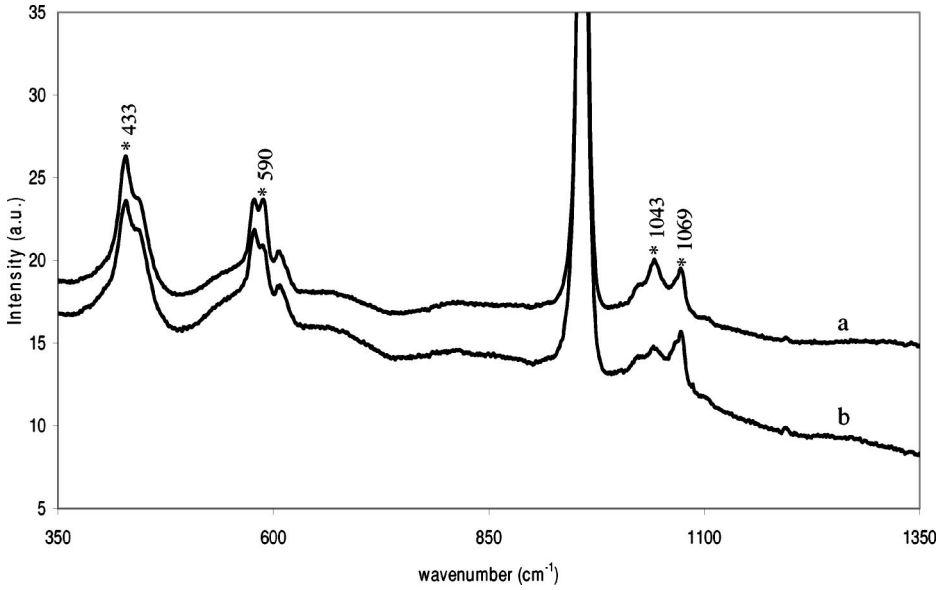

Fig. 10 Representative fiber-optic Raman spectra (not corrected for luminescence background) of (a) carious enamel and (b) sound enamel acquired with an InPhotonics Raman probe for 830 nm laser excitation. Spectra were normalized to the 959 cm^{-1} peak and were offset for clarity.

ered by the current OCT system is approximately 1 mm across. Although a small range, this is sufficient to probe the approximately 2 mm×2 mm area found below (gingival to) the contact points of adjacent teeth where such interproximal caries develop. OCT can therefore be used to sweep across this region to rapidly identify possible early carious sites as well as to determine the lesion depth. Based upon OCT morphological guidance, Raman spectroscopy can then be used to examine the suspected lesion to provide biochemical information. For example, a Raman probe can be used to sample various points along the OCT imaging line. Then based upon the ratios of the various Raman peaks, it can be determined rapidly whether the region exhibits spectral properties indicative of (early) carious enamel and distinguished from sound enamel. The Raman data therefore confirms the scattering aberration detected by OCT to be a carious lesion. The combination of both techniques overcomes the limitation of using each technique alone leading to results of better sensitivity and specificity.

In order to examine the reproducibility of fiber-optic Raman spectroscopy for caries characterization, multiple-point measurements were acquired along a line on a tooth surface containing two carious lesions. The same lesion was previously examined by OCT and shown in Fig. 4(B). Figure 12(A) highlights the points sampled (shaded dots shown on the image in a linear fashion) and Fig. 12(B) shows the re-

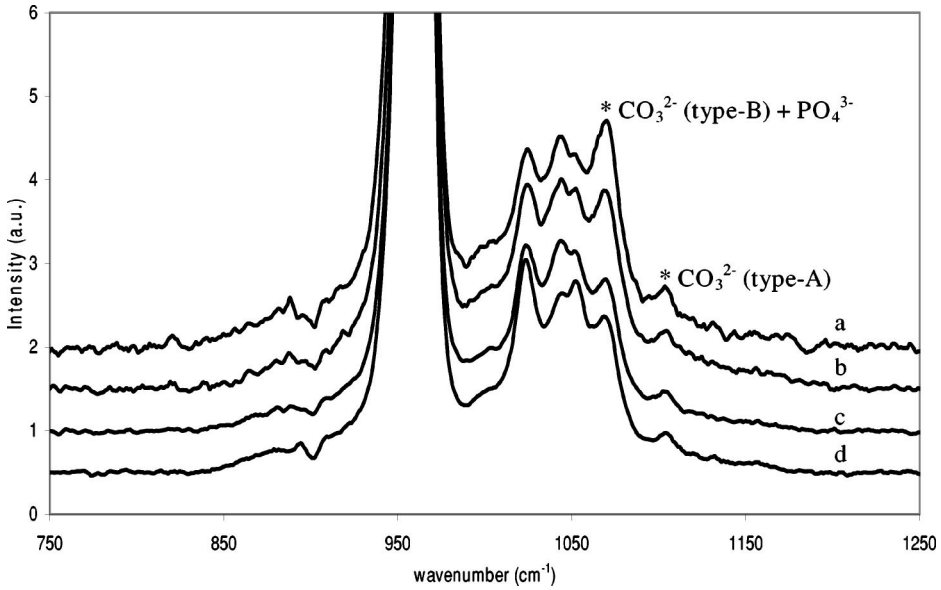

Fig. 11 Representative Raman microspectroscopic spectra in the 750–1200 cm^{-1} region of sound enamel measured with (a) ×5, (b) ×10, (c) ×50 and (d) ×100 microscope objectives.

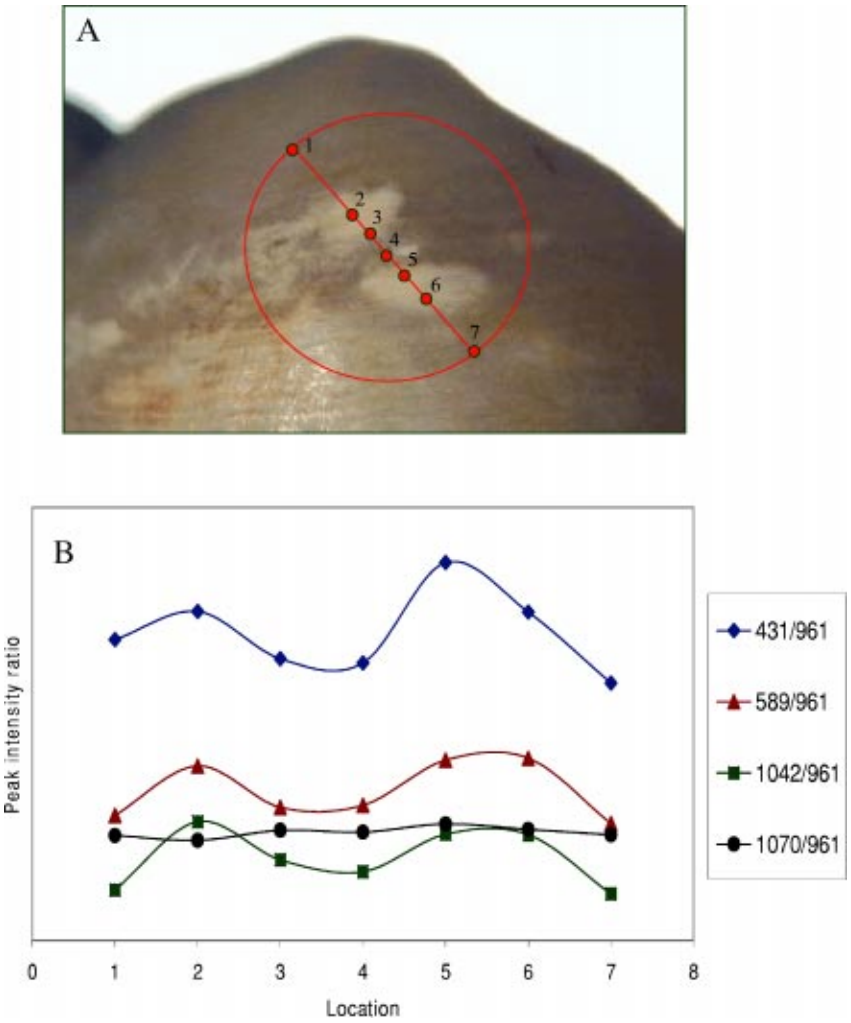

Fig. 12 (A) Photomicrograph of a tooth surface containing two carious lesions (white areas). Shaded dots represent actual Raman sampling locations with a fiber-optic Raman probe. (B) Intensity ratio plot of various Raman peaks (431, 589, 1042, and 1070 cm^{-1}) relative to the 961 cm^{-1} peak corresponding to the sampling locations shown in (A).

spective intensity ratio of various peaks relative to the $\nu_1 PO_4^{3-}$ peak at each sampling location. The increased intensity ratio correlates well with the locations of the carious lesions, as previously observed with the microspectroscopic study [see Fig. 7(B)]. These findings also correspond well with the OCT imaging where regions of carious lesions demonstrated increased light backscattering intensity. Therefore, the spectroscopic contrast between the carious and sound enamel present in the microscopic spectra is largely preserved in the fiber-optic measurements. This observation supports the possibility of transferring this technology from a lab bench study to a clinical application.

4 Conclusion

Our studies have demonstrated that optical coherence tomographic imaging of incipient dental caries results in increased light backscattering intensity in a triangular-shaped region below the enamel surface suggestive of demineralization during caries development. The OCT images also provide an estimate of the carious lesion depth. Further, we have shown that near-IR Raman microspectroscopy and fiber-optic Raman spectroscopy are useful for characterizing early dental caries. Sound enamel can be distinguished from carious enamel based on changes of various Raman band intensities arising from PO_4^{3-} of hydroxyapatite within mineralized tissue. The local ultrastructural and morphological changes induced by the de-/remineralization activities during caries development give rise to the spectral changes observed. In particular, the loss of the original symmetry and/or orientation of the enamel apatite crystallites within the demineralized zone as a result of mineral dissolution may be responsible for the observed changes. Preliminary polarized Raman spectroscopic studies have provided evidence to support this hypothesis.

Good correlation has been demonstrated between the OCT images with Raman spectral and imaging data for caries detection and characterization. At lesion sites where OCT reveals deeper light penetration and stronger scattering indicative of a highly porous structure, Raman spectroscopic changes characteristic of enamel structural alterations were also observed to confirm demineralization. We have shown that by combining the strengths of both OCT and Raman spectroscopic techniques, a new optical method for early

enamel caries detection can be developed. Further, the use of specialized fiber-optic probes will provide improved access to the interproximal region compared to conventional diagnostic tools. The advantage of using OCT for *in vivo* caries detection is facilitated with a probe device. The white spot lesions described for the current studies were observed upon *ex vivo* visual inspection by two clinicians. Prior to extraction, the white spot lesions are at the interproximal regions. Since these lesions are not visible because they are blocked by the adjacent tooth, the lesion is often not diagnosed by the dentist. A probe that accesses the proximal surfaces would allow OCT screening for incipient caries. Merely having a visible imaging fibre to obtain a direct visual image of the interproximal region is not necessarily sufficient to detect white spot lesions. This is because the early white spot lesion is usually observed with the assistance of air-drying the tooth surface. Such lesions are more difficult to observe when wet. For the current application, OCT provides the same overall information about the presence or absence of a carious lesion regardless of a wet or air-dried surface. OCT would therefore help locate early dental caries and provide depth information, a parameter which is not available from visual inspection of intact teeth but which is important for clinical treatment decisions. Using Raman spectroscopy with OCT would furnish biochemical specificity of the presence of demineralization and confirm the results suggested by OCT. Further, with Raman spectroscopy, semiquantitative measures of the extent of demineralization can be obtained. From a clinical viewpoint, this information would be useful to the dentist in helping determine treatment strategies such as deciding to surgically restore the lesion (if at the advanced stage) or to promote remineralization and monitor the carious site over time. The nonionizing nature of these multimodal optical methods will also allow for frequent patient monitoring and thus improving the quality of dental health care.

Acknowledgments

Partial funding was received from a grant from the Manitoba Medical Service Foundation and from the National Research Council Canada's Genomics and Health Initiative. The authors thank Dr. Colin Dawes (Dept. of Oral Biology, Faculty of Dentistry, University of Manitoba) for useful discussions on cariology.

References

1. Anonymous, ''Diagnosis and management of dental caries throughout life. National Institutes of Health Consensus Development Conference statement, March 26–28, 2001,'' *J. Dent. Educ.* **65**, 1162–1168 (2001).
2. U.S. Department of Health and Human Services, ''Oral health in America: A report of the Surgeon General—executive summary,'' U.S. Department of Health and Human Services, National Institute of Dental and Craniofacial Research, National Institutes of Health, Rockville, MD (2000).
3. G. K. Stookey, R. D. Jackson, A. G. Zandona, and M. Analoui, ''Dental caries diagnosis,'' *Dent. Clin. North Am.* **43**, 665–677 (1999).
4. G. K. Stookey and C. Conzalez-Cabezas, ''Emerging methods of caries diagnosis,'' *J. Dent. Educ.* **65**, 1001–1006 (2001).
5. C. A. Murdoch-Kinch, ''Oral medicine: advances in diagnostic procedures,'' *J. Calif. Dent. Assoc.* **27**, 773–780 (1999).
6. A. Hall and J. M. Girkin, ''A review of potential new diagnostic modalities for caries lesions,'' *J. Dent. Res.* **83**, C89–C94 (2004).
7. A. Schneiderman, M. Elbaum, T. Shultz, S. Keem, M. Greenebaum, and J. Driller, ''Assessment of dental caries with digital imaging fiber-optic transillumination (DIFOTI): in vitro study,'' *Caries Res.* **31**, 103–110 (1997).
8. B. T. Amaechi and S. M. Higham, ''Quantitative light-induced fluorescence: A potential tool for general dental assessment,'' *J. Biomed. Opt.* **7**, 7–13 (2002).
9. X. Q. Shi, U. Welander, and B. Angmar-Mansson, ''Occlusal caries detection with KaVo DIAGNOdent and radiography: an in vitro comparison,'' *Caries Res.* **34**, 151–158 (2000).
10. A. Lussi, B. Megert, C. Longbottom, E. Reich, and P. Francescut, ''Clinical performance of a laser fluorescence device for detection of occlusal caries lesions,'' *Eur. J. Oral Sci.* **109**, 14–19 (2001).
11. C. Robinson, R. C. Shore, S. J. Brookes, S. Strafford, S. R. Wood, and J. Kirkham, ''The chemistry of enamel caries,'' *Crit. Rev. Oral Biol. Med.* **11**, 481–495 (2000).
12. L. M. Silverstone, ''Structure of carious enamel, including the early lesion,'' *Oral Sci. Rev.* **3**, 100–160 (1973).
13. D. J. White, ''The application of in vitro models to research on demineralizaton and remineralizatoin of the teeth,'' *Adv. Dent. Res.* **9**, 175–193 (1995).
14. F. I. Feldchtein, G. V. Gelikonov, V. M. Gelikonov, R. R. Iksanov, R. V. Kuranov, A. M. Sergeev, N. D. Gladkova, M. N. Ourutina, J. A. Warren, Jr., and D. H. Reitze, ''In vivo OCT imaging of hard and soft tissue of the oral cavity,'' *Opt. Express* **3**, 239–250 (1998).
15. A. Baumgartner, S. Dichtl, C. K. Hitzenberger, H. Sattmann, B. Robl, A. Moritz, A. F. Fercher, and W. Sperr, ''Polarization-sensitive optical coherence tomography of dental structures,'' *Caries Res.* **34**, 59–69 (2000).
16. B. W. Colston, Jr., M. J. Everett, U. S. Sathyam, L. B. DaSilva, and L. L. Otis, ''Imaging of the oral cavity using optical coherence tomography,'' *Monogr. Oral Sci.* **17**, 32–55 (2000).
17. B. T. Amaechi, S. M. Higham, A. G. Podoleanu, J. A. Rogers, and D. A. Jackson, ''Use of optical coherence tomography for assessment of dental caries: quantitative procedure,'' *J. Oral Rehabil.* **28**, 1092–1093 (2001).
18. C. K. Hitzenberger, E. Gotzinger, M. Sticker, M. Pircher, and A. F. Fercher, ''Measurement and imaging of birefringence and optic axis orientation by phase resolved polarization sensitive optical coherence tomography,'' *Opt. Express* **9**, 780–790 (2001).
19. D. Fried, J. Xie, S. Shafi, J. D. B. Featherstone, T. M. Breunig, and C. Le, ''Imaging carious lesions and lesion progression with polarization sensitive optical coherence tomography,'' *J. Biomed. Opt.* **7**, 618–627 (2002).
20. E. B. Hanlon, R. Manoharan, T. W. Koo, K. E. Shafer, J. T. Motz, M. Fitzmaurice, J. R. Kramer, I. Itzkan, R. Dasari, and M. Feld, ''Prospects for in vivo Raman spectroscopy,'' *Phys. Med. Biol.* **45**, R1–R59 (2000).
21. H. Tsuda and J. Arends, ''Raman spectroscopy in dental research: a short review of recent studies,'' *Adv. Dent. Res.* **11**, 539–547 (1997).
22. M. T. Kirchner, H. G. M. Edwards, D. Lucy, and A. M. Pollard, ''Ancient and modern specimens of human teeth: a Fourier transform Raman spectroscopic study,'' *J. Raman Spectrosc.* **28**, 171–178 (1997).
23. S. Stewart, D. A. Shea, C. P. Tarnowski, M. D. Morris, D. Wang, R. Franceschi, D.-L. Lin, and E. Keller, ''Trends in early mineralization of murine calvarial osteoblastic cultures: a Raman microscopic study,'' *J. Raman Spectrosc.* **33**, 536–543 (2002).
24. A. Carden and M. D. Morris, ''Application of vibrational spectroscopy to the study of mineralized tissues (review),'' *J. Biomed. Opt.* **5**, 259–268 (2000).
25. A. Carden, R. M. Rajachar, M. D. Morris, and D. H. Kohn, ''Ultrastructural changes accompanying the mechanical deformation of bone tissue: A Raman imaging study,'' *Calcif. Tissue Int.* **72**, 166–175 (2003).
26. J. A. Timlin, A. Carden, and M. D. Morris, ''Raman spectroscopic imaging markers for fatigue-related microdamage in bovine bone,'' *Anal. Chem.* **72**, 2229–2236 (2000).
27. H. Ou-Yang, E. P. Paschalis, A. L. Boskey, and R. Mendelsohn, ''Two-dimensional vibrational correlation spectroscopy of *in vitro* hydroxyapatite maturation,'' *Biopolymers* **57**, 129–139 (2000).
28. Y. Leung and M. D. Morris, ''Characterization of the effects of postextraction treatments on human dentin-resin interface by micro-Raman spectroscopy,'' *J. Biomed. Opt.* **2**, 120–124 (1997).
29. E. Wentrup-Byrne, C. A. Armstrong, R. S. Armstrong, and B. M. Collins, ''Fourier transform Raman microscopic mapping of molecular components in a human tooth,'' *J. Raman Spectrosc.* **28**, 151–158 (1997).

30. P. Tramini, B. Pelissier, J. Valcarcel, B. Bonnet, and L. Maury, ''A Raman spectroscopic investigation of dentin and enamel structures modified by lactic acid,'' *Caries Res.* **34**, 233–240 (2000).
31. J. Xu, I. Stangel, I. S. Butler, and D. F. R. Gilson, ''An FT-Raman spectroscopic investigation of dentin and collagen surfaces modified by 2-hydroxyethylmethacrylate,'' *J. Dent. Res.* **76**, 596–601 (1997).
32. R. M. Lemor, M. B. Kruger, D. M. Wieliezka, J. R. Swafford, and P. Spencer, ''Spectroscopic and morphologic characterization of the dentin/adhesive interface,'' *J. Biomed. Opt.* **4**, 22–27 (1999).
33. R. Lemor, M. B. Kruger, D. M. Wieliczka, P. Spencer, and T. May, ''Dentin etch chemistry investigated by Raman and infrared spectroscopy,'' *J. Raman Spectrosc.* **31**, 171–176 (2000).
34. P. Spencer, Y. Wang, M. P. Walker, D. M. Wieliczka, and J. R. Swafford, ''Interfacial chemistry of the dentin/adhesive bond,'' *J. Dent. Res.* **79**, 1458–1463 (2000).
35. B. van Meerbeek, H. Mohrbacker, J. P. Celis, J. R. Roos, M. Braem, P. Lambrechts, and G. Vanherle, ''Chemical characatization of the resin-dentin interface by micro-Raman spectroscopy,'' *J. Dent. Res.* **72**, 1423–1428 (1993).
36. H. Tsuda and J. Arends, ''Orientational micro-Raman spectroscopy on hydroxyapatite single crystals and human enamel crystallites,'' *J. Dent. Res.* **73**, 1703–1710 (1994).
37. G. Leroy, G. Penel, N. Leroy, and E. Brès, ''Human tooth enamel: a Raman polarized approach,'' *Appl. Spectrosc.* **56**, 1030–1034 (2002).
38. W. Hill and V. Petrou, ''Detection of caries and composite resin restorations by near-infrared Raman spectroscopy,'' *Appl. Spectrosc.* **51**, 1265–1268 (1997).
39. W. Hill and V. Petrou, ''Caries detection by diode laser Raman spectroscopy,'' *Appl. Spectrosc.* **54**, 795–799 (2000).
40. D. Fried, R. E. Glena, J. D. B. Featherstone, and W. Seka, ''Nature of light scattering in dental enamel and dentin at visible and near-infrared wavelengths,'' *Appl. Opt.* **34**, 1278–1285 (1995).
41. E. S. Etz, W. S. Hurst, and S. J. Choquette, ''Raman intensity calibration with glass luminescence standards,'' *Inst. Phys. Conf. Ser.* **165**, 121–122 (2000).
42. K. G. Ray and R. L. McCreery, ''Simplified calibration of instrument response function for Raman spectrometers based on luminescent intensity standards,'' *Appl. Spectrosc.* **51**, 108–116 (1997).
43. K. J. Frost and R. L. McCreery, ''Calibration of Raman spectrometer instrument response function with luminescence standards: An update,'' *Appl. Spectrosc.* **52**, 1614–1618 (1998).
44. G. Penel, G. Leroy, C. Rey, and E. Brès, ''MicroRaman spectral study of the PO_4 and CO_3 vibrational modes in synthetic and biological apatites,'' *Calcif. Tissue Int.* **63**, 475–481 (1998).
45. J. J. Freeman, B. Wopenka, M. J. Silva, and J. D. Pasteris, ''Raman spectroscopic detection of changes in bioapatite in mouse femora as a function of age and *in vitro* fluoride treatment,'' *Calcif. Tissue Int.* **68**, 156–162 (2001).
46. J. D. Pasteris, B. Wopenka, J. J. Freeman, K. Rogers, E. Valsami-Jones, J. A. M. van der Houwen, and M. J. Silva, ''Lack of OH in nanocrystalline apatite as a function of degree of atomic order: implications for bone and biomaterials,'' *Biomaterials* **25**, 229–238 (2004).
47. R. Z. LeGeros, ''Chemical and cystallographical events in the caries process,'' *J. Dent. Res.* **69**, 567–574 (1990).
48. F. F. M. de Mul, M. H. J. Hottenhuis, P. Bouter, J. Greve, J. Arends, and J. J. ten Bosch, ''Micro-Raman line broadening in synthetic carbonated hydroxyapatite,'' *J. Dent. Res.* **65**, 437–440 (1986).
49. C. Robinson, J. A. Weatherell, and J. Kirkham, ''The chemistry of dental caries,'' in *Dental Enamel: Formation to Destruction*, C. Robinson, J. Kirkham, and R. Shore, Eds., pp. 223–243, CRC Press Inc., Boca Raton, FL (1995).
50. A. S. Hallsworth and C. Robinson, ''Loss of carbonate during the first stages of enamel caries,'' *Caries Res.* **7**, 345–348 (1973).
51. C. Robinson, J. A. Weatherell, and A. S. Hallsworth, ''Alterations in the composition of permanent human enamel during caries attack,'' in *Demineralisation and Remineralisation of the Teeth*, S. A. Leach and W. M. Edgar, Eds., IRL Press, Oxford, p. 209 (1983).
52. J. C. Elliot, ''Mineral, synthetic and biological carbonate apatites,'' in *Structure and Chemistry of the Apatites and Other Calcium Orthophosphates*, pp. 191–304, Elsevier, New York (1994).
53. J. A. Weatherell, C. Robinson, and C. R. Hiller, ''Distribution of carbonate in thin sections of dental enamel,'' *Caries Res.* **2**, 1–9 (1968).